ELSEVIER

Journal of Structural Geology 30 (2008) 65–80

JOURNAL OF STRUCTURAL GEOLOGY

www.elsevier.com/locate/jsg

# Recess drawn by the internal zone outer boundary and oblique structures in the paleomargin-derived units (Subbetic Domain, central Betics): An analogue modelling approach

Ana Crespo-Blanc*

*Departamento de Geodinámica, Instituto Andaluz de Ciencias de la Tierra, Universidad de Granada – CSIC, 18071 Granada, Spain*

Received 30 March 2007; received in revised form 18 July 2007; accepted 5 September 2007
Available online 2 October 2007

**Abstract**

The Subbetic Domain, comprising the South Iberian paleomargin-derived units, is a fold-and-thrust belt developed over a ductile substrate showing a complex structural pattern. In the central Betics, a main trend can be defined, with respect to which frequent oblique structures are observed. These oblique structures, often subperpendicular to the main trend, are not located along transfer zones but rather are present everywhere in the fold-and-thrust belt. Moreover, they are coetaneous with those drawing the main trend. This complex pattern is situated in front of a recess marked by the outer boundary of the internal zones – the Alboran Domain – which acted as backstop. Analogue models were designed to study the influence of such a recess on a ductile-brittle multilayer. One of the models, in which the backstop recess is symmetric with respect to its direction of movement, shows a high variation in the orientation of the resulting structures, being not only qualitatively but also quantitatively similar to the studied natural case.
© 2007 Elsevier Ltd. All rights reserved.

*Keywords:* Betics; Structural pattern; Oblique structures; Ductile substrate; Recess; Analogue modelling

## 1. Introduction

The Alpine-Mediterranean orogenic belt, and in particular the Gibraltar Arc area, is generally known as a case study of extensional processes that went hand in hand with compressional ones. During the Miocene, the Betic-Rif orogen was affected by rifting in the internal part of the Gibraltar Arc, while folding and thrusting took place in its external part (Platt and Vissers, 1989; Frizon de Lamotte et al., 1991; García-Dueñas et al., 1992). Over the past two decades, much attention has been paid to the extensional processes that affected the Alboran Domain, that is, the internal zones common to both branches of the Gibraltar Arc (see review in Frizon de Lamotte et al., 2004). In contrast, only a few papers address the structural evolution of the external zones, namely the External Rif and Subbetic Domains, respectively, south and north of the Gibraltar Strait. Within the Subbetic units of the central Betics, Crespo-Blanc (2007) recently described a very complex fold-and-thrust geometry resulting from Early to Middle Miocene shortening. Oblique structures with respect to the main structural trend are frequent, most notably in an area where the external–internal zone boundary draws a recess. Superposed buckle folding has also been described for the same area (Crespo-Blanc, 2007). The present paper sheds some light on the various hypotheses that may be put forth regarding the formation of such oblique structures – which are distributed throughout the area, and not located along transfer zones – by applying the analogue modelling tool.

The analogue experiments presented in this paper help to broaden the available experimental templates for natural thrust wedges. Together with a review of previously published analogue models, they allow us to test whether a simple recess of the backstop geometry might be evoked to explain the genesis of oblique structures in a tectonic domain thus far poorly understood from a structural point of view.

* Tel.: +34 58244030; fax: +34 58248527.
*E-mail address:* acrespo@ugr.es

0191-8141/$ - see front matter © 2007 Elsevier Ltd. All rights reserved.
doi:10.1016/j.jsg.2007.09.009

## 2. The Betic-Rif orogenic wedge

The Betic and Rif arc-shaped mountain belt around the Strait of Gibraltar closes, to the west, the Alpine-Mediterranean orogenic system, which developed during the late Mesozoic to Cenozoic convergence between Africa and Iberia. Various tectonic domains can be differentiated around the Gibraltar Arc (Fig. 1). The South Iberian and Maghrebian paleomargin-derived units consist of autochthonous, parautochthonous and/or allochthonous non-metamorphic Mesozoic and Tertiary covers. They respectively detached during Miocene times from a Variscan basement, the Iberian Meseta and the Moroccan Meseta, and now constitute the Prebetic and Subbetic Domains in Spain, and the Pre-Rif, Meso-Rif and Intra-Rif Domains in

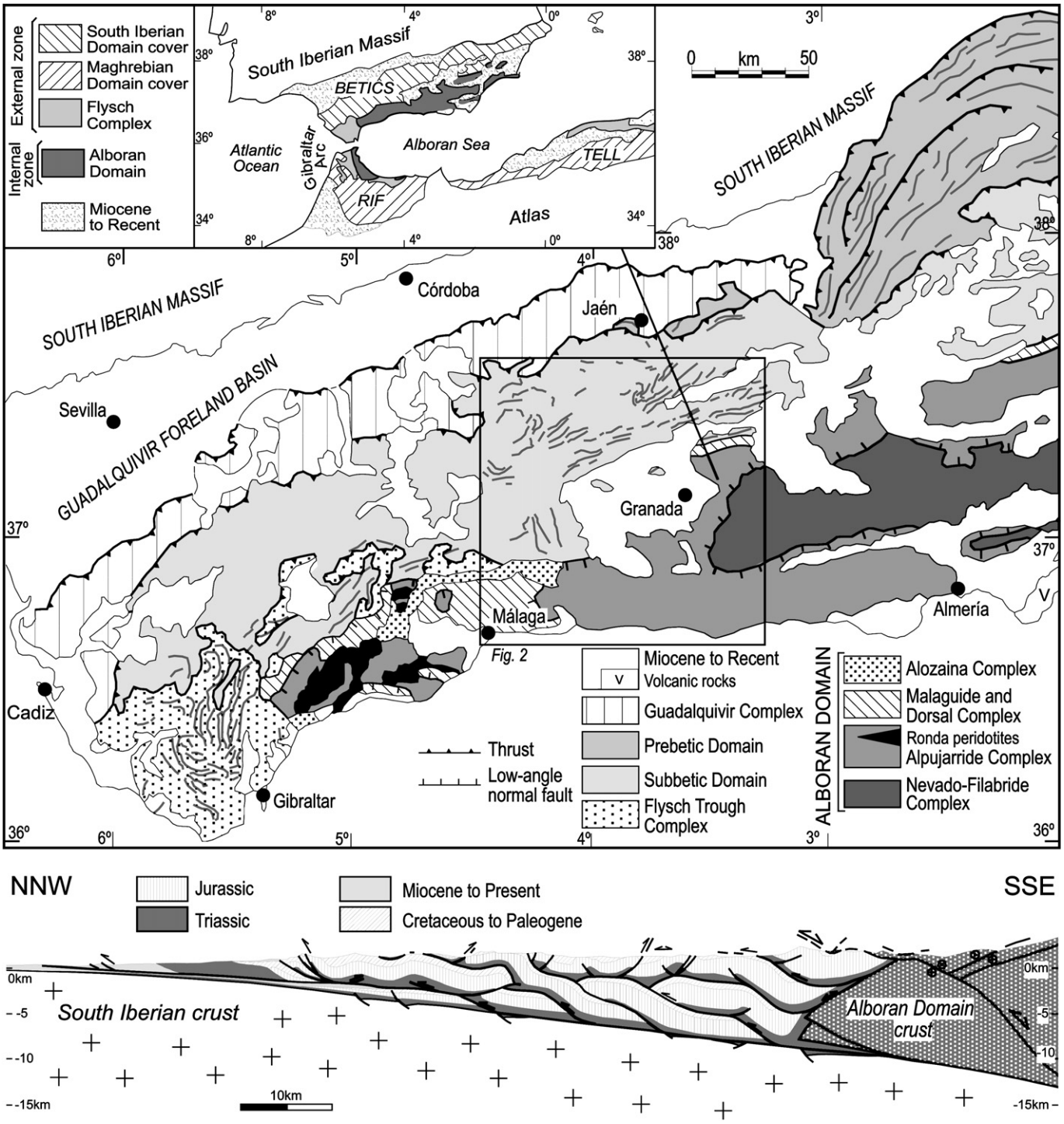


Fig. 1. Tectonic map of the Subbetic Domain in the central and western Betics (northern branch of the Gibraltar Arc) and trend of the structures associated with the main shortening. Large-scale cross-section (located on the map) according to Frizon de Lamotte et al. (2004). Inset: Alpine orogenic belts in the westernmost Mediterranean region.

Morocco. The Flysch Trough Units, presently located in the western Betics and along the northern part of Africa from the Strait of Gibraltar to Tunisia (inset of Fig. 1), derived from a basin with attenuated/oceanic crust overlain by Jurassic to Miocene deep-water sediments (Biju-Duval et al., 1978; Dercourt et al., 1986; Durand-Delga et al., 2000). They separate the internal zone from the paleomargin-derived units. The Alboran Crustal Domain, a predominantly metamorphic hinterland formed mainly by Palaeozoic to Triassic rocks, represents the relics of a former Alpine orogenic wedge that was stretched and drifted apart during the Neogene extensional episodes (Balanyá and García-Dueñas, 1988; Comas et al., 1999). It occupies the inner part of the Gibraltar Arc and conforms the basement of the Alboran Basin.

Shortening in front of the Gibraltar Arc was due to the westward migration of the Alboran Domain from Oligocene to Miocene times. It produced the obliteration of the Flysch Trough, and the detachment and thrust stacking of its Upper Jurassic to Miocene siliciclastic infill. The migration of compression was responsible for the inclusion of the sedimentary covers of the South Iberian and Maghrebian paleomargins into the deformed wedge, and the corresponding development of foredeep and foreland basins (Guadalquivir and Rharb Basins, respectively) (Balanyá and García-Dueñas, 1988; Lonergan and White, 1997; Frizon de Lamotte et al., 2004). Meanwhile shortening took place in the external zones *sensu lato*, in the back-arc, rifting and crustal extension affected the whole Alboran Domain. Extensional fault systems developed, leading to the Alboran Basin formation (Comas et al., 1992, 1999; García-Dueñas et al., 1992). Finally, from Late Tortonian to Pliocene times, the Alboran region underwent continuous N–S to NW–SE compression (Weijermars et al., 1985; Comas et al., 1999; Balanyá et al., 2007).

## 3. Main features of the evolution of South Iberian paleomargin-derived units

The cover of the South Iberian paleomargin is made up of sedimentary, non-metamorphosed rocks. Meanwhile, the Late Triassic is represented by claystones with gypsum and fine-grained sandstones (Keuper facies), and the Jurassic to Neogene sequences are formed by carbonate rocks. At the beginning of the Jurassic, a broad shallow-marine environment developed. This carbonate platform broke down at the end of the Early Jurassic, leading to the differentiation of the Subbetic and Prebetic Zones from that time onwards (Fig. 1). Whereas the Prebetic Zone is characterized by shallow-water facies – with continental deposits and/or erosional episodes – pelagic facies prevail in the Subbetic Zone (García-Hernández et al., 1980; Vera, 2004). In the latter, the External, Median and Internal Subbetic Zones have been distinguished. Their areal distribution in the central Betics appears in Fig. 2. This differentiation was made on the basis of paleogeographic criteria and their position with respect to the emerged Variscan basement; the Median Subbetic is the most subsiding realm during Jurassic times, but the Cretaceous is uniformly developed for the three Zones (García-Hernández et al., 1980; Vera, 2004). The synthetic lithostratigraphic columns of the sequences that belong to the Internal and Median Subbetic Domain, respectively, and which are involved in part of the central Betic fold-and-thrust belt are drawn in Fig. 3.

Due to the collision between the internal and the external domains, the South Iberian paleomargin units detached mainly along the Keuper facies formation. Shortening produced folding, thrusting and nappe-stacking whose structural trend appears in Fig. 1. The timing of the structural evolution of the paleomargin-derived units varies from one part to the other of the Betics. In general, deformation is more recent towards the external part and towards the west. In the Subbetic Domain of the central Betics, the main folds and thrusts developed close to the Aquitanian–Burdigalian transition (Crespo-Blanc, 2007). In the western Betics, however (from meridian 4.5° to the west), the external zones *sensu lato*, represented by both the Subbetic Domain and the Flysch Trough Complex, were deformed mainly during Late Burdigalian times (Crespo-Blanc and Campos, 2001).

The large-scale cross-section of Fig. 1, based on Frizon de Lamotte et al. (2004), illustrates the structural style of the Subbetic Domain in the central Betics, which consists of large slices thrusted mainly according to a piggy-back sequence. At first glance it would appear to correspond to a simple fold-and-thrust wedge developed over a ductile substrate, yet a zoom in on the orientation and distribution of the structures of this area will reveal that this image more complex in map view (Fig. 2).

## 4. Central Betics: structural trend in the Subbetic fold-and-thrust belt and timing of the deformation

In the central Betics, the internal structure of the Subbetic units can be chaotic, due to the low strength of the evaporitic rocks that represent the substrate of the thrust slices. Accordingly, the Subbetic Domain has been differentiated into ''structured'' and ''chaotic'' Subbetics (Vera, 2004). The trend of the folds and thrusts within the structured Subbetic Domain is mainly NE–SW to ENE–WSW directed (Fig. 2). Nevertheless, in many areas, oblique structures – that is, structures whose orientation differs from the main trend – and superposed buckle folding can be found.

The most spectacular oblique structures are the NNE–SSW structures situated 50 km ENE of Granada, in the Sierra Gorda area (Figs.1 and 2), but these are not the only ones. A careful examination of Fig. 2 shows that 10 km W of Iznájar, 10 km S and SE of Priego, 15 km W and 5 km NNE of Priego, 20 km NW of Alcalá la Real, and 12 km NW of Campillos some folds and/or thrusts are oblique with respect to the main trend, or even perpendicular to it. Moreover, the superposed folding W of Priego and SW of Campillos is very distinctive of the Subbetic Domain in the central Betics, as described in detail by Crespo-Blanc (2007). It should be stressed that all these anomalously trending structures are not alineated or located along a transfer zone. Rather, they are randomly distributed over the entire area of Fig. 2. This is a very characteristic feature of the central Betic external zones.

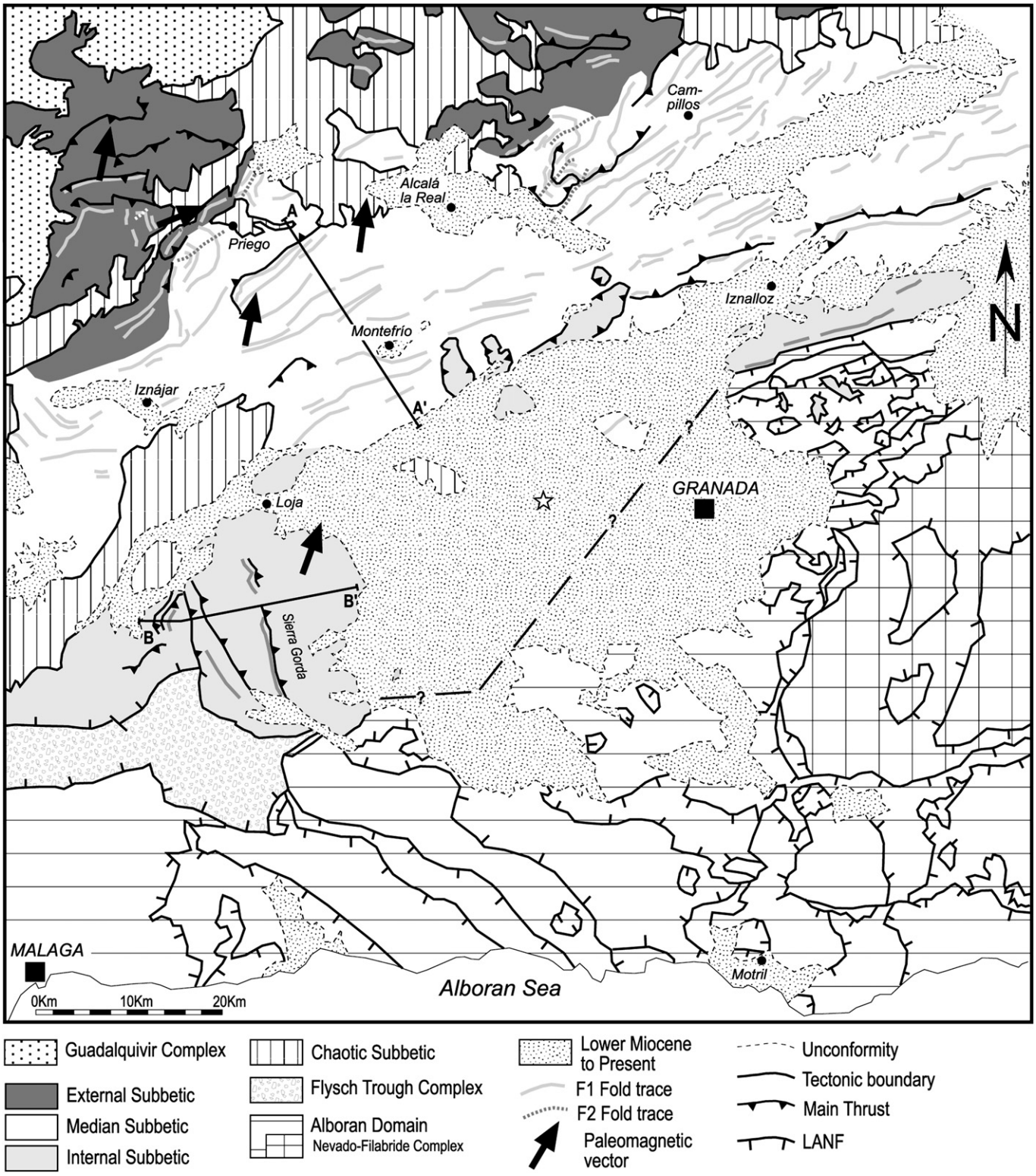


Fig. 2. Simplified structural map with the trend of the folds and thrusts associated with the main shortening within the Internal, Median and External Subbetic Domains cropping out in the central Betics (localization on Fig. 1). It shows the recess drawn by the Subbetic and Alboran Domain boundary. Paleomagnetic remagnetization vector according to Osete et al. (2004). ☆ – Commercial well at the bottom of which Subbetic materials were drilled.

One of the key questions behind any working hypothesis about the origin of such oblique structures is that of determining their timing with respect to the ENE–WSW-trending folds and thrusts that define the main structural trend. Although the latter developed close to the Aquitanian–Burdigalian transition (Crespo-Blanc, 2007), very few age constraints exist for the oblique structures or fold interferences. For example, the NNW–SSE-trending thrust imbrication of Sierra Gorda is

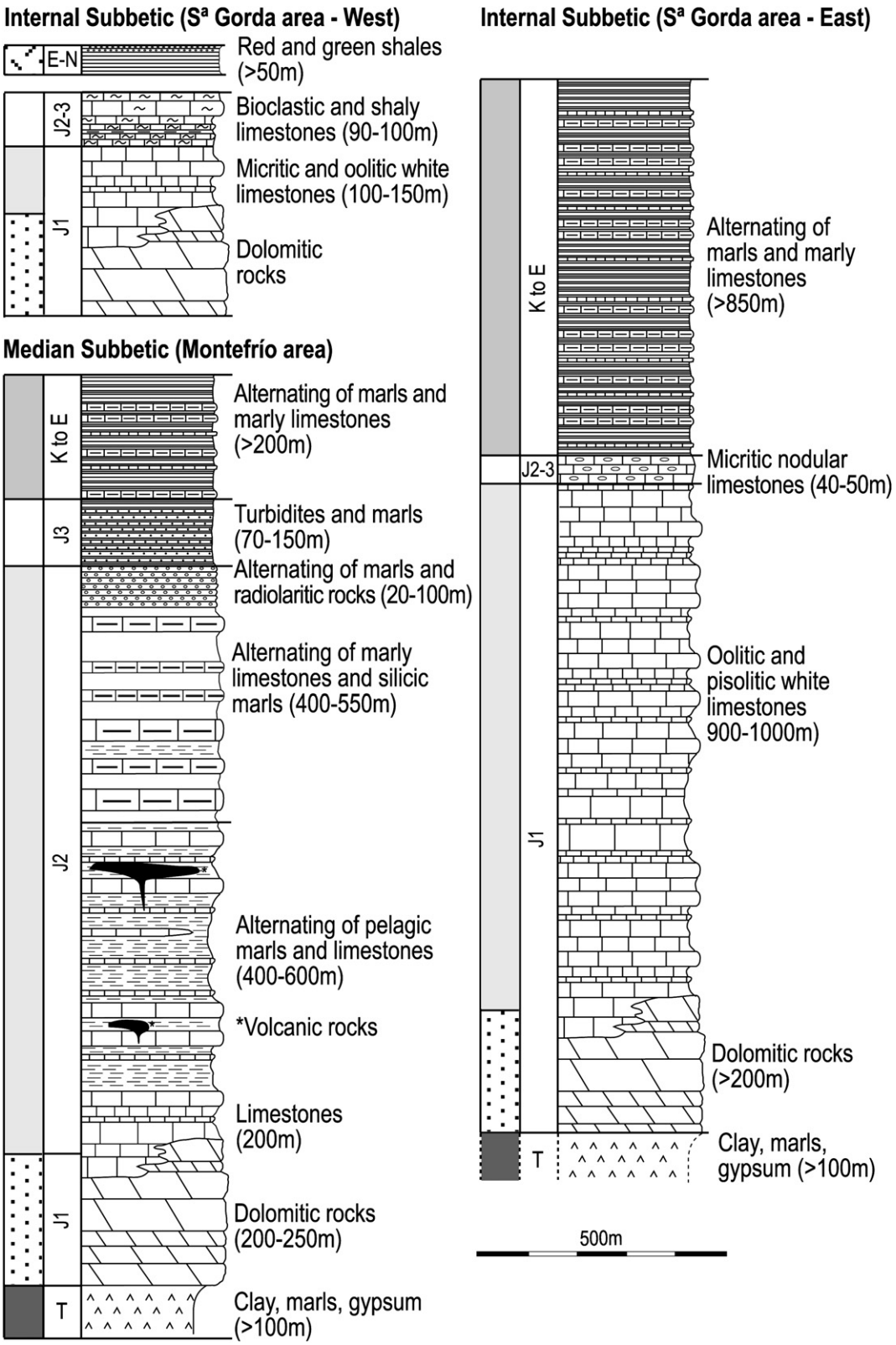


Fig. 3. Synthetic lithostratigraphic succession of the Subbetic units in the areas where the cross-sections of Fig. 4 have been drawn. The column belonging to the Median Subbetic Domain (cross-section A–A′ of Fig. 4) has been drawn according to Lupiani et al. (1988a) and Díaz de Neira et al. (1991) and own data. The columns of Sierra Gorda area belongs to the Internal Subbetic Domain (cross-section B–B′ of Fig. 4) and has been drawn according to Lupiani et al. (1988b), Pineda and Ruiz (1983) and own data. The column named "S$^{a}$ Gorda area (East)" corresponds with the lithostratigraphy of the two thrust sheets situated in the eastern part of the cross-section. Abbreviations in the lithostratigraphic columns: T, Triassic; J. Jurassic (Subscripts 1, 2 and 3: Lower, Median and Upper, respectively); K, Cretaceous; E: Paleogene; N: Ne.

sealed by Tortonian subhorizontal sedimentary rocks cropping out east and north of Sierra Gorda (Lupiani et al., 1988a,b), and the age interval of the formation of this thrust system spans over the whole Early and Middle Miocene. Consequently, other types of data are needed to constrain the relative age of the structures. Paleomagnetic data show that a widespread secondary remagnetization event took place during Neogene times (Villalaín et al., 1994; Osete et al., 2004). Structural and regional data, through a comparison of the rotations of the paleomagnetic vectors and the age of deformation in the central and western Subbetic, restrict the time interval of the remagnetization event to the Burdigalian (Crespo-Blanc, 2007). In the area of Fig. 2, this remagnetization was imprinted upon the Subbetic deformed wedge, as the orientation of the remagnetization vector is clearly independent of the structural trend. Both in the ENE–WSW-directed fold-and-thrusts that draw the normal trend, and in the oblique NNW–SSE directed structures of Sierra Gorda, it shows a constant, very slightly clockwise rotated orientation. Only one sampling site, a few kilometers west of Priego, is rotated due to superposed folding (see full discussion in Crespo-Blanc, 2007). It is thus assumed that the folds and thrusts with normal trend as well as those which are oblique developed within a very short time span, if not coetaneously.

## 5. Structural style of the Subbetic Domain fold-and-thrust belt

Two detailed cross-sections of the uppermost thrust sheet of the Subbetic units are presented in Fig. 4. Cross-section A–A′ is NW–SE oriented, that is subperpendicular to the main structural trend; while cross-section B–B′ is WSW–-ENE oriented, as it crosses the area situated south of Loja where the trend is anomalously directed (Fig. 2).

The deformation style of the folds and thrusts is controlled by the rheology of the lithostratigraphic sequences involved, shown synthetically in Fig. 3. Cross-section A–A′ shows an almost 20 km long thrust sheet composed by – from bottom to top – a low strength decollement layer of evaporitic rocks (over 100 m thick) cropping out in the northern part of the cross-section, a competent layer of dolomitic rocks (around 250 m thick), and a less competent layer of alternating marls, marly limestones and limestones (1000–1500 m thick, Figs. 3 and 4). This thrust sheet, which draws a box fold accompanied by smooth folds, is bounded to the NNW by a pop-up and to the SSE by a pop-down structure (Fig. 4). Such a lack of preferred vergence is characteristic of many areas of the structured Subbetic Domain, and is due to the presence of the weak layer of evaporites as substrate of the fold-and-thrust system.

It must be stressed that the structural style characterized by cross-section A–A′ is common to the whole Subbetic units outcropping in the central Betics. In particular, it also characterizes the oblique structures and the folds involved in the interferences. By contrast, cross-section B–B′, orthogonal to the NNW–SSE-trending oblique structures, shows a well-defined W to WSW vergence (Fig. 4). It is defined by a thrust system whose western part is characterized by two huge thrust sheets around 10 km long, whereas in the eastern part of the cross-section, much shorter thrust slices appear (less than 1 km). This striking difference is related with the thickness of the involved lithostratigraphic sequence. To the west, it is very thin (around 450 m) and is made up of a very competent unit of massive carbonate rocks overlain by competent limestones (“Sierra Gorda area-West” of Fig. 3). Atop it, incompetent shales can be found. To the east, a very competent unit of dolostones and limestones appears, with a thickness reaching at least 1200 m. It is overlain by a 700 m-thick, less competent unit of alternating marls and marly limestones (“Sierra Gorda area-East” of Fig. 3). Hence, one should take note that the basal detachment of the thrust system does not reach the surface (Fig. 4). Triassic evaporitic rocks are nevertheless present very near the western end of the cross-section, in the so-called “chaotic Subbetic” (Fig. 2), though not directly observed at the bottom of the thrust sheet. Such weak rocks are also present below the internal Subbetic situated northeast of Granada. Accordingly, it is probable that although the well-defined vergence is more characteristic of a brittle substrate, the thrust system of Sierra Gorda area developed over ductile evaporites.

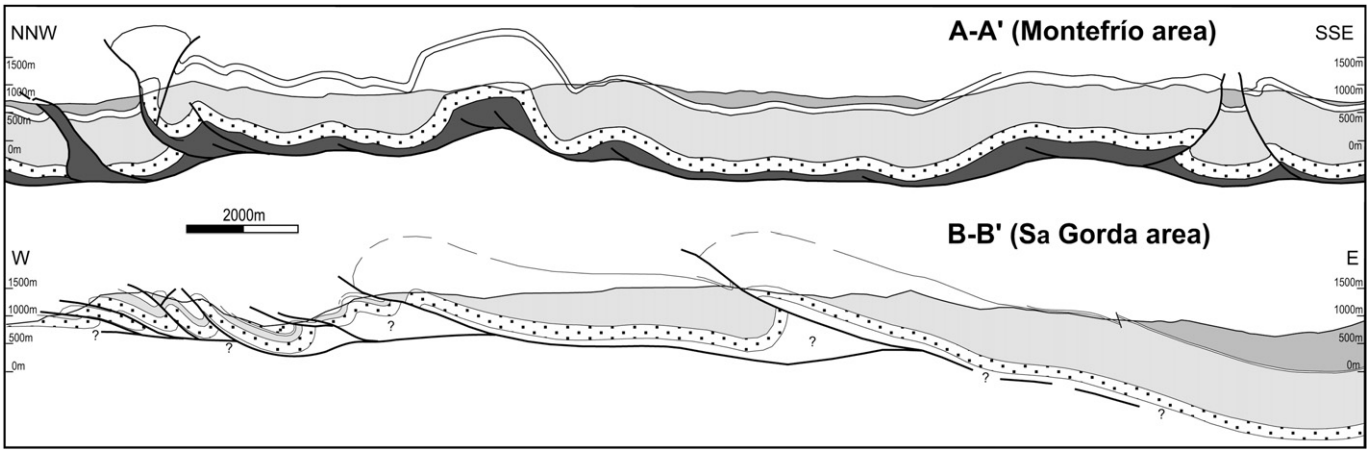


Fig. 4. Detailed cross-sections characteristic of the structural style of the Subbetic Units in the central Betics. (A) Montefrío area and (B) Sierra Gorda area. The legend of the cross-sections appears in Fig. 3, to the left of the lithostratigraphic columns. Localization of the cross-sections on Fig. 2.

## 6. Oblique structures in the Subbetic Domain of the central Betics: are they related with a backstop recess?

The origin of oblique structures in a deformed wedge may be related to: (i) an along-strike displacement gradient (Hindle and Burkhard, 1999), (ii) heterogeneities in the basement geometry (Mansy et al., 2003), (iii) heterogeneities in the folded sequence (Corrado et al., 1998; Soto et al., 2002, 2003), (iv) heterogeneities in the substrate (Bahroudi and Koyi, 2003; Luján et al., 2003; Affolter and Gratier, 2004) and/or (v) the salients and recesses of the backstop (Calassou et al., 1993; Kley, 1999; Macedo and Marshak, 1999; Likorish et al., 2002).

In the studied natural case of the oblique fold and thrust of the central Subbetic, an along-strike displacement gradient can be immediately ruled out, as we are not dealing with an arcuate fold-and-thrust belt, but with oblique structures that punctuate the whole Subbetic Domain. Heterogeneities in the basement geometry can also be immediately ruled out, because this is the uppermost thrust sheet of the Subbetic wedge, and the basement is situated below several very thick thrust sheets (see cross-section of Fig. 1). Heterogeneities in the folded sequence have been evidenced only in the Sierra Gorda thrust system, its western part showing a decrease in thickness with respect to its eastern part (Fig. 3); in other area of the central Betics, the rheological properties of the folded and thrusted sequence are similar. Heterogeneities in the substrate (thickness or brittle-ductile rheology) cannot be ruled out since, for example, Triassic evaporites below the Sierra Gorda thrust system are not directly observed (see previous epigraph).

As for salients or recesses of the backstop, it is worth noting that the irregularity of the trend lines of the structures developed in the Subbetic Domain is particularly pronounced in front of a recess marked by the Alboran Domain outer boundary. This boundary is oriented approximately E–W to ENE–WSW in the central Betics – that is, parallel with the main structural trend of the Subbetic Domain – although it draws an N–S gap of about 30 km in the area of Fig. 2. This boundary sometimes disappears below Miocene to Recent deposits around Granada, but commercial well data can be used to constrain its approximate geometry. Indeed, at the bottom of Granada D1 well (star on Fig. 2), Subbetic materials were drilled (Rodríguez-Fernández and Sanz de Galdeano, 2006).

The geometry of this recess is tentatively sketched in Fig. 2 (see also Fig. 10). It must be stressed that the eastern branch of this recess, which has been drawn as a straight line, could also be interpreted as the envelope of ENE–WSW-trending segments of the internal external zone boundary, displaced by a system of dextral, approximately N–S-trending strike-slip faults. Nevertheless, such faults are not observed around or within the Granada Basin, N–S-trending strike-slip faults are present, they are mainly dextral.

Bearing this in mind, the complex pattern of the structures in the Subbetic units in the central Betics will be interpreted in terms of oblique structures developed in front of a backstop recess, in a fold-and-thrust belt that developed over an evaporitic substrate. In particular, the most important oblique structures in the Subbetic units, the N–S to NNW–SSE thrust system situated south of Loja, are contiguous to the Alboran Domain and are located in the western branch of this recess. This hypothesis will be tested through an analogue modelling approach.

## 7. Folding and thrusting in the central Subbetic Domain: convergence velocity and strain rate estimations

In order to achieve adequate scaling between the natural case and analogue modelling, convergence velocity and strain rate must be estimated. In the central Betics, the relationships between the Miocene deposits of the piggy-back basins and the structured Subbetic units show that the main shortening, which generated NE–SW to ENE–WSW-directed folds and thrusts, took place close to the Aquitanian–Burdigalian transition, although tightening of the pre-existing structures occurred during Middle and Late Miocene (Crespo-Blanc, 2007). The age of the foredeep olistostromic deposits, which derived from the erosion of reliefs associated with the active mountain front, evidences a migration of the main deformation from SSE to NNW. Indeed, these deposits are Early Burdigalian in age in the southernmost part of the central Subbetic domain (18.8–20.5 Ma according to Berggren et al., 1985), and Serravallian in age in the northernmost outcrops (14.8–11.2 Ma, Berggren et al., 1985) (Comas, 1978; Vera, 2000). If it is assumed that deformation took place during the same time interval, shortening developed in a 9.3–4.0 Ma time interval. On the other hand, a total shortening within the Subbetic units of 91 km can be roughly estimated from the large-scale cross-section along the central Betics (Fig. 1). In this cross-section, the initial and final lengths of the uppermost level of Jurassic rocks are 155 and 64 km, respectively. Accordingly, a convergence velocity of 1.0–2.3 cm/year ($3.1 \times 10^{-10}$ to $7.2 \times 10^{-10}$ ms$^{-1}$) can be estimated, that is, a strain rate of $4.8–11.3 \times 10^{-15}$ s$^{-1}$.

## 8. An analogue modelling approach: backstop recess and ductile-brittle multilayer

### 8.1. Material properties, scaling and model set up

In the experiments, sand and silicone were used as analogue materials in a natural gravity field to simulate the brittle behaviour of upper crustal sedimentary rocks (Davy and Cobbold, 1991) and the ductile flow of evaporitic rocks (Weijermars et al., 1993; Cotton and Koyi, 2000; Bonini, 2001), respectively. Dry quartz sand was used, with a grain size varying between 0.2 and 0.3 mm, a coefficient of internal friction $\phi = 37°$, and density $\rho_{bM} = 1.77$ g/cm$^3$. Coloured sand provided horizontal passive markers within the undeformed experimental multilayer. The silicone putty used in our experiments (transparent Rhodosil Gum FB of Rhone-Poulenc) is a Newtonian material, with a density $\rho_{dM} = 0.98$ g cm$^{-3}$ and a viscosity $\eta_M = 0.5 \times 10^5$ Pa s at room temperature (Funiciello et al., 2003). A constant shortening rate of $1.74 \times 10^{-6}$ m s$^{-1}$ (0.63 cm h$^{-1}$) was imposed in all the models.

Table 1
Scaling parameters between nature and model

| Parameter | Nature (N) | Model (M) | Scaling factor (N/M) |
|---|---|---|---|
| Length $l$ (m) | $1 \times 10^3$ | $5 \times 10^{-3}$ | $2 \times 10^5$ |
| Density $\rho_v$ (kg m$^{-3}$) | 2200(a,b) | 980 | 2.24 |
| Density $\rho_b$ (kg m$^{-3}$) | 2400(b,c) | 1770 | 1.35 |
| Density contrast $\rho_b/\rho_v$ | 1.1 | 1.8 | – |
| Viscosity $\eta$ (Pa s) | $0.1 \times 10^{18}$(d) to $10 \times 10^{18}$(b) | $0.5 \times 10^5$ | $0.2 \times 10^{12}$ to $20 \times 10^{12}$ |
| Convergence velocity $v$ (m s$^{-1}$) | $3.1 \times 10^{-10}$ to $7.2 \times 10^{-10}$(1.0–2.3 cm/year) | $1.74 \times 10^{-6}$(0.63 cm h$^{-1}$) | $1.78 \times 10^{-4}$ |

(a) Weijermars et al. (1993); (b) Koyi (1988); (c) Cotton and Koyi (2000).

Table 1 shows the characteristic values of the density ($\rho$), length ($l$), viscosity ($\eta$) and velocity ($v$) for both natural case and analogue materials. The table also shows the relative scaling factors of the main physical parameters. With the chosen velocity of convergence in the model, (a) under natural gravity conditions ($g_N = g_M = 9.81$ m s$^{-2}$), (b) assuming a length ratio ($l_N/l_M$) of $2 \times 10^5$ (1 cm in experiments represented 2000 m in nature), and (c) according to the approach of Weijermars and Schmeling (1986), where $v_N = \frac{\eta_M}{\eta_N}\left(\frac{\rho_{dN} g_N l_N^2}{\rho_{dM} g_M l_M^2}\right) v_M$, the viscosity of the evaporitic horizons should correspond to the highest viscosities given by Cotton and Koyi (2000), as $\eta_N$ calculated according to this formula gives values of $1.1–2.5 \times 10^{19}$ Pa s.

The experiments were performed in a sandbox schematically illustrated in Fig. 5. The multilayer was built in the recess of a rigid backstop whose geometry varied from one model to the other. The angle marked by the recess was of 90° or 120°, and the movement of the backstop was parallel to the symmetry axis of this angle (Models 90-45 and 120-22) or oblique with respect to it, its perpendicular drawing either an angle of 30° (Model 90-30) or an angle of 0° with one of the sides of the backstop (Model 120-0) (Fig. 5).

The pre-deformational configuration of the experimental multilayer was identical in all models, and the rheological stratification consisted of (i) an upper brittle layer composed of alternating layers of coloured and uncoloured dry sand (1 cm thick), and (ii) a lower ductile layer of silicone putty (0.5 cm thick) (Fig. 5). In addition, Model 90-45Sand was performed with a multilayer composed only by sand, a backstop recess of 90° and a movement of the backstop parallel to the symmetry axis.

A 4 cm-side grid was sieved on top of the multilayer. A mylar sheet floored the sandbox, and sand was used to confine the whole model. Pushing the rigid backstop attached to a motor drive caused collision of the multilayers against it, and the consequent growth of the fold-and-thrust wedges. The amount of total movement of the backstop was approximately 20 cm in all experiments. The evolution of the experiments was recorded by time-lapse photographs of the top surface. After completion, each model was wetted with water and serially sectioned parallel to the convergence direction.

All the experiments were performed in the Analogue Modelling Laboratory of the Geodynamics Department of the University of Granada (Spain).

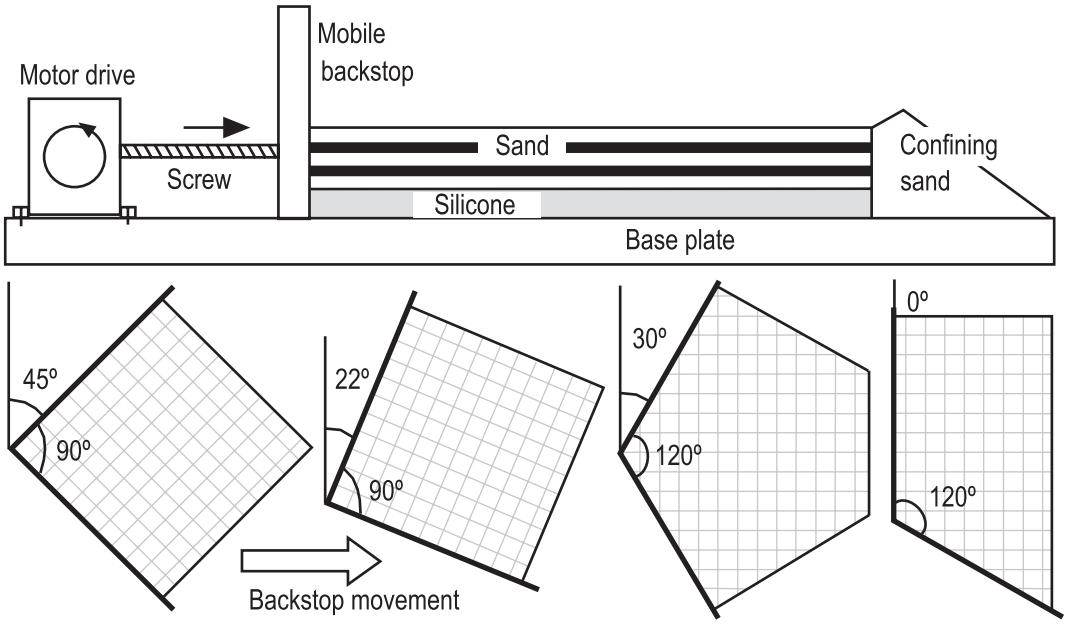


Fig. 5. Simplified sketch of the experimental apparatus and model setting in both cross-section and map view. The geometry of the backstop in the different experiments is schematically illustrated (Models 90-45, 90-22. 120-30 and 120-0, from left to right).

### 8.2. Experimental results: progressive evolution of the thrust wedge

The progression of deformation of each of the multilayer models is illustrated by a series of line drawing from overhead photographs (Figs. 6–9). In the final experimental stage, the numbers indicate the nucleation sequence of the thrusts. Some of the thrusts that developed in the first stages were totally covered by slice thrusts later; when this occurred, their sequence numbering appears in one of the progressive stage line drawings.

In all models, deformation started with a thrust that mimicked the outer boundary of the experimental multilayer. This border effect is neglected in the description which follows. When shortening proceeded, the sandpack above the ductile substrate was deformed mainly by box folds. They were bounded by both forward and rearward vergent thrusts and/or kink bands, which developed almost simultaneously. The resulting geometry shows a very low surface wedge taper enhanced by the lack of dominant vergence. The photograph of Fig. 6B shows a representative cross-section that illustrates the finite 2D geometry. It can also be seen how the pop-down structures sank into the silicone and were, in some cases, totally covered by subsequent thrust slices (Fig. 8A). Indeed, buoyancy-driven processes are enhanced in the models with respect to the natural case, as the density contrast between

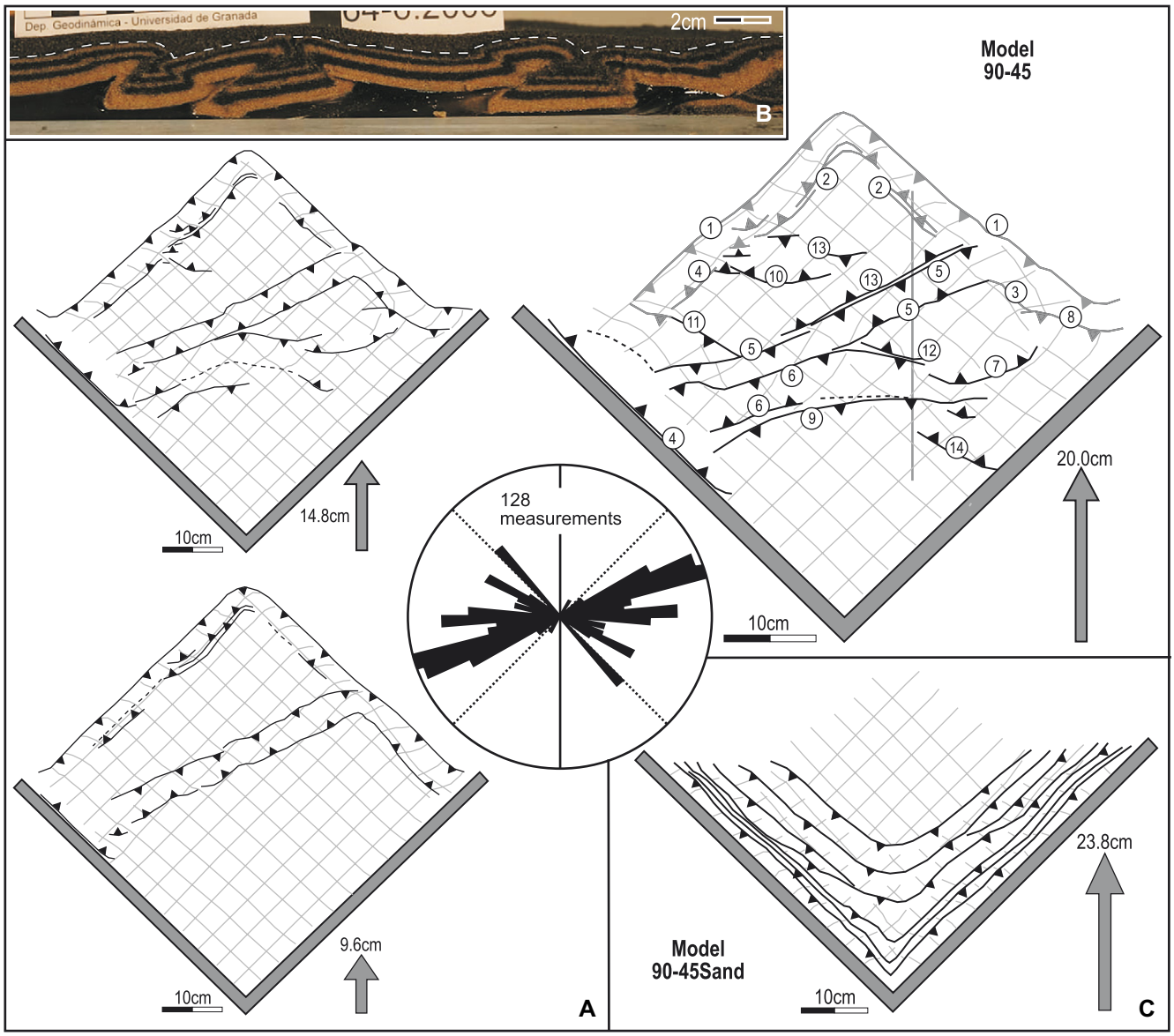


Fig. 6. (A) Line drawings of map view of Model 90-45 for various amounts of shortening indicated as total movement of the backstop in centimetres (drawn from photographs). In the final stage line drawing, the numbers indicate the nucleation sequence of the faults. In order to represent their orientation, the structure traces were divided into 2 cm long segments, measured with respect to the movement of the backstop and plotted in the rose diagram (total measurements: 128; largest petal: 17 values). The thrust which formed in the outer part of the models (border effect) were not considered (thrusts in grey in the final stage line drawing). The dotted lines in the rose diagram represent the backstop side orientation. (B) Photograph of a cross-section representative of the structural style of the experimental wedges (located as a straight line in the final stage line drawing). (C) Line drawing of final stage map view of Model 90-45Sand.

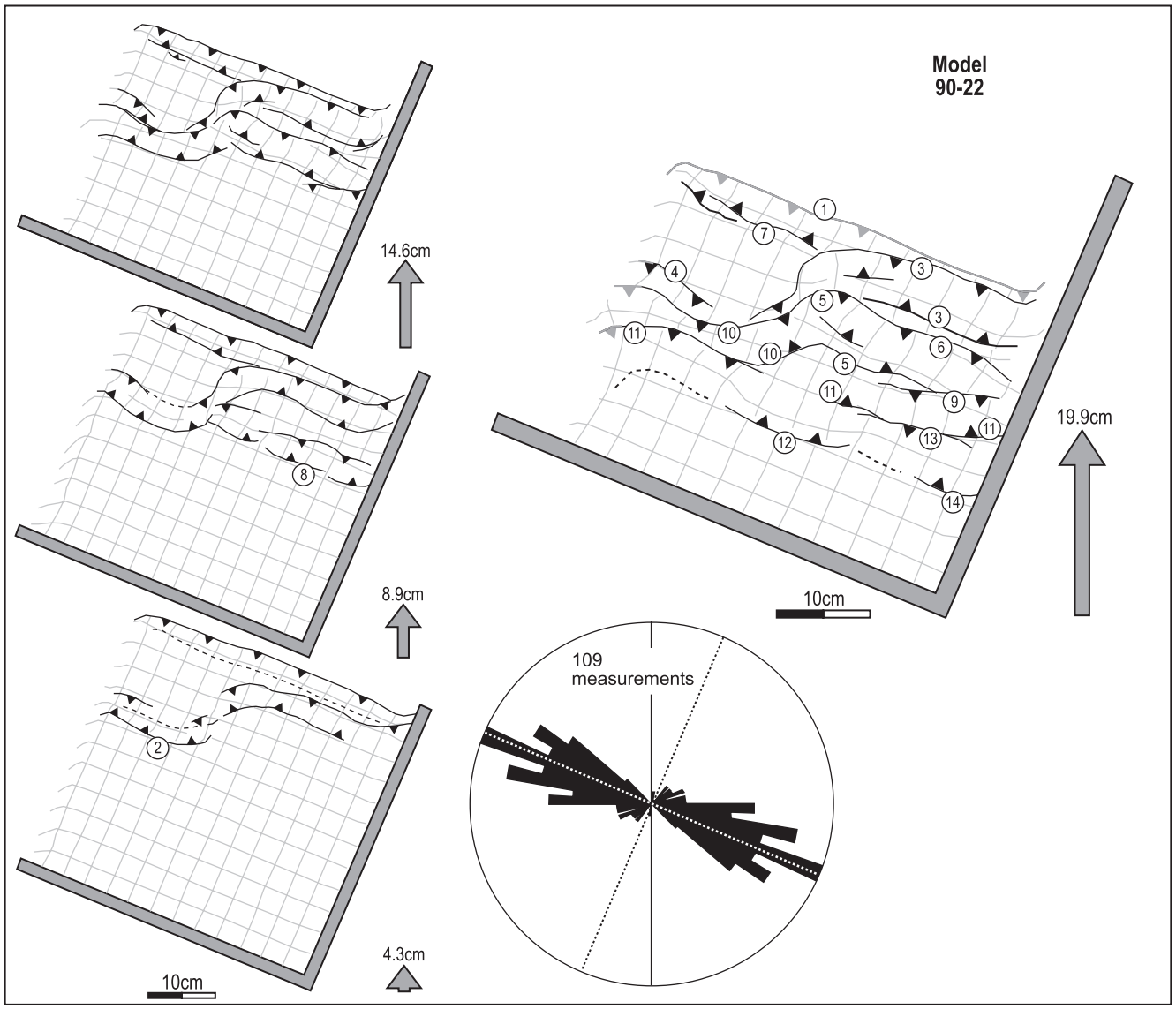


Fig. 7. Line drawings of map view of Model 90-22 for various amounts of shortening indicated as total movement of the backstop in centimetres (redrawn from photographs). See rest of legend concerning the numbers and the rose diagram in Fig. 6A. Rose diagram: total measurements, 109; largest petal, 16 values.

the brittle and the ductile layer of the model is almost twice that existing between the carbonate sequence and the evaporitic layer in nature (Table 1).

The first structure that developed in Model 90-45, after the border effect, is a box fold bounded by thrusts that run straight from one part to the other of the multilayer in the central sector of the model (Fig. 6). This box fold is neither parallel nor perpendicular to the backstop movement or to any of the recess sides. As shortening proceeded, other non-cylindrical pairs of box folds, accompanied by their corresponding forward and rearward vergent thrusts, developed. They nucleate without following any rule of propagation in terms of pattern of occurrence, as they first developed in the rear part of the model (thrusts 6, 7 and 9 of Fig. 6) and then in the frontal one (thrusts 10, 11 and 13).

The first stage of Model 90-22 is characterized by the development of an S-shaped structure that links two pairs of forward and rearward vergent thrusts. This pair of thrusts is parallel to the recess side, at a higher angle with respect to the one perpendicular to the backstop movement (Fig. 7). When shortening proceeded, most of the structures developed in the internal part of the model with respect to this S-shaped structure, nearly parallel to the same recess side, though slightly sinuous (e.g. thrusts 9, 11–13). A second pair of thrusts mimics the first S-shaped structure (thrust 10).

In the first stage of Model 120-30, an arc-shaped box fold bounded by both forward and rearward vergent thrusts developed in the centre of the multilayer (Fig. 8). It shows the same concavity as the backstop recess, and its lateral branches are slightly oblique with respect to the backstop sides. When shortening proceeded, this structure was slightly squeezed in map view and its lateral branches reached parallelism with the backstop sides. Then, two other arcuate structures developed, convex with respect to the backstop recess, one of

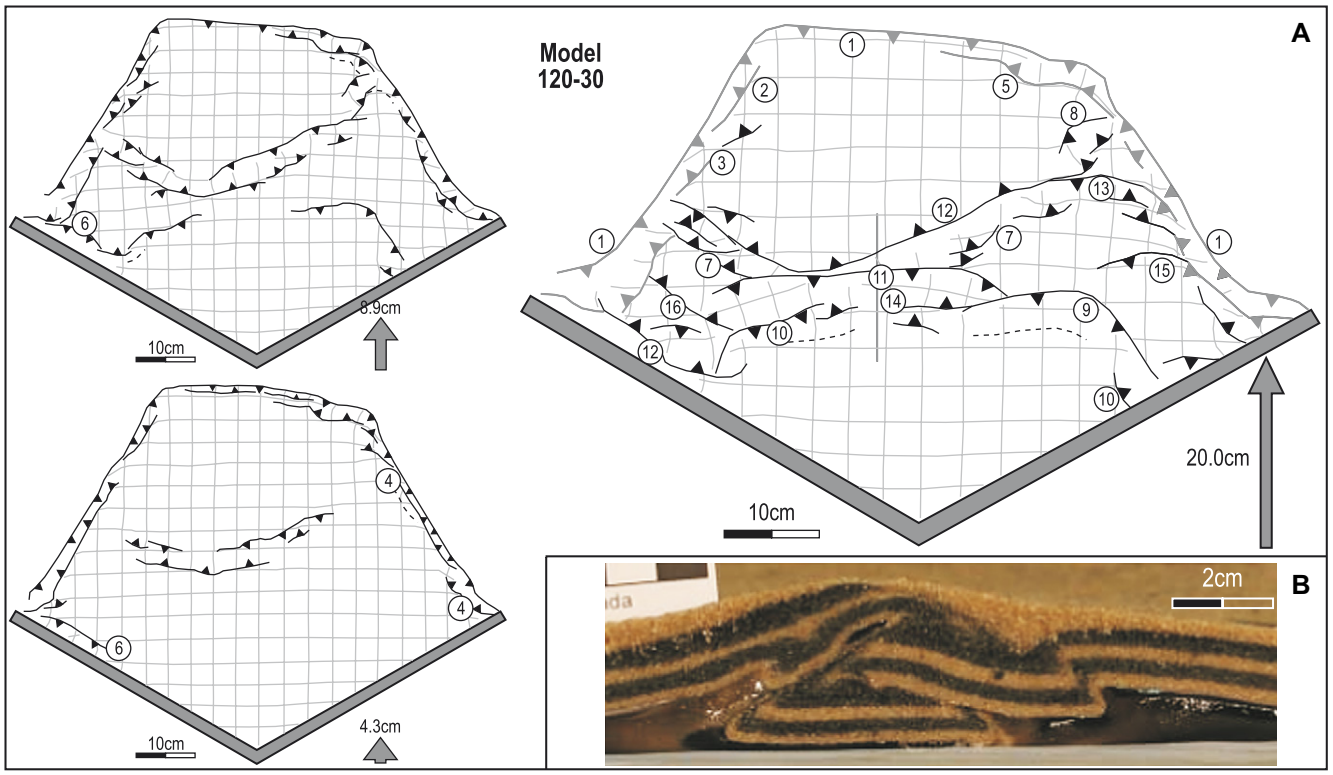


Fig. 8. (A) Line drawings of map view of Model 120-30 for various amounts of shortening indicated as total movement of the backstop in centimetres (redrawn from photographs). In the final stage line drawing, the numbers indicate the nucleation sequence of the faults. Thrusts 4 and 6, indicated in previous stages, were hidden below late thrust. The corresponding rose diagram appears in Fig. 10. (B) Photograph of a cross-section showing a pop-down syncline sunk in the silicone and covered by a subsequent thrust slice (localized as a straight line in the final stage line drawing).

them closer than the other (thrusts 9 and 10 of Fig. 8). Finally, deformation was mainly concentrated in the central part of the model, where an intense shortening took place. It caused the disappearance of a pop-down that sank into the silicone. Then, this pop-down was thrusted by another thrust sheet (Fig. 8B).

Model 120-0 can be considered the most cylindrical model of all the experiments (Fig. 9). At the beginning of this modelling, the folds and thrusts were only slightly sinuous, with a general trend subparallel to the side of the recess that is perpendicular to the backstop movement. A general propagation of the deformation toward the external part of the model took place. At the final stage, the box folds that developed near the oblique side of the recess are seen to be slightly rotated (counterclockwise), drawing a small angle with respect to the recess side perpendicular to the backstop movement.

The structural deformation style observed in the multilayer floored by silicone strongly contrasts with that made up only of sand (Model 90-45Sand; Fig. 6C). The latter showed a typical piggy-back sequence evolution of the thrust wedge. Deformation was concentrated at the front of the wedge, and two systems of almost rectilinear thrusts developed parallel to the backstop sides. These were linked by a transfer zone situated along the symmetry plane of the backstop recess. The result of this experiment closely resembles that of Calassou et al. (1993), who describe a sandpack pushed by a backstop with a recess of 145°, and with one side perpendicular to the backstop movement (sketch of Fig. 9B). In their case, the thrust systems are also parallel to the backstop sides.

### *8.3. Final geometry: main structural trend and oblique structures*

The analogue models presented in this paper developed non-cylindrical structures and a complex structural pattern: a main trend can be defined, and, relative to it, frequent oblique structures are observed. Again, we stress that these oblique structures developed everywhere in the model and were not located along discrete transfer zones. Moreover, the structures are coetaneous, regardless of their orientation.

The spatial distribution of the structures and their grade of obliquity can be quantified through rose diagrams. In the line drawing of the final stage, the structure lines were divided into segments of 2 cm length, and their mean orientation was measured. The north of the rose diagrams corresponds to the backstop movement direction, while each petal represents an interval of 5° of strike orientation. It must be stressed that the folds and thrusts situated in the outer boundary of the multilayer were neglected (border effect). These diagrams appear in parallel with the model line drawings (Figs. 6, 7 and 9), except that corresponding to Model 120-30, drawn in Fig. 10.

Model 120-0 shows a very well defined main trend as well as the lowest grade of obliquity (Fig. 9). Some 95% of the orientation measurements range in a 50° interval (between N65E

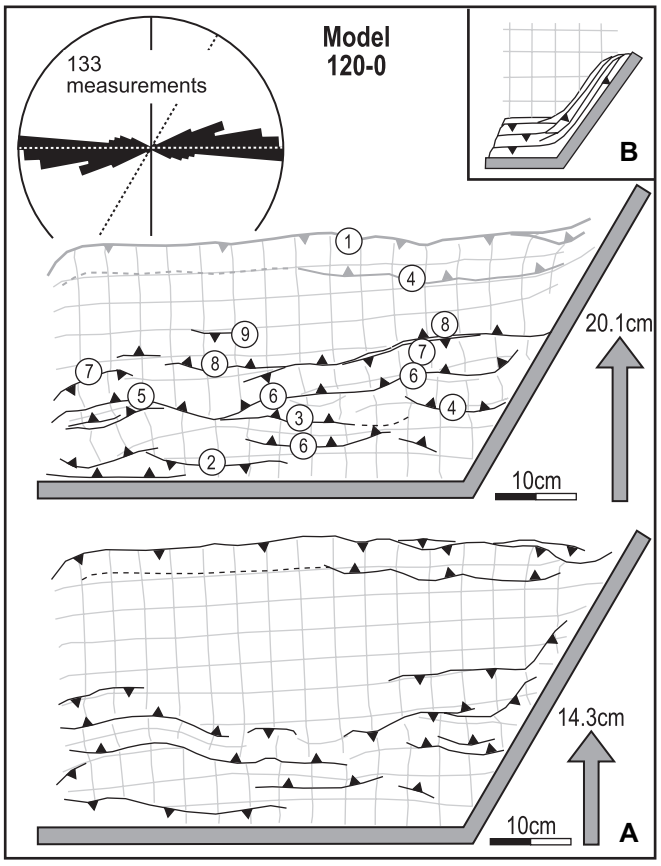


Fig. 9. (A) Line drawings of map view of Model 120-0. See rest of legend concerning the numbers and the rose diagram in Fig. 6A. Rose diagram: total measurements, 133; largest petal, 25 values. (B) Line drawings of map view of a model realized by Calassou et al. (1993), a sandpack shortened by a backstop with a recess of 145° and with one of its side perpendicular to the backstop movement.

and N115E) and 52% of the values are comprised within a 15° range, between N80E and N95E. The mean orientation N86E is almost perpendicular to the backstop movement.

Despite the pronounced S-shaped structures that formed at the beginning of the experiment, Model 90-22 shows a marked main trend and a minor amount of oblique structures, with 82% of the measurements between N90E and 130E (40° range); the mean orientation of the structures is N103E, that is, subparallel to the backstop recess side that produced most of the shortening in the multilayer (Fig. 7).

The rose diagrams of Models 90-45 and 120-30 (Figs. 6 and 10, respectively) show the highest variation of the orientation of the structures. Although the mean trend of the structures is almost parallel to the perpendicular to the backstop movement (N87E and N94E, respectively), a pronounced variation of the orientation can be observed. Indeed, in both experiments, most of the measurements vary between N60E and N140E. Moreover, a 40° range (between N60E and 100E) comprises only 67% or 55% of the measurements (Models 90-45 and 120-30, respectively).

In summary, models in which the backstop recess is symmetric with respect to its movement show the highest variation in orientation of the resulting structures. Furthermore, if the movement is asymmetric, with one of the entrant sides at higher angle with respect to the backstop movement, it favours the development of folds and thrusts nearly parallel to this particular side.

## 9. Discussion

### *9.1. Oblique structure development: backstop recess vs other initial model configurations*

The models presented in this paper provide insights as to the kinematics and mode of development of folds and thrusts in a situation of backstop recess with a ductile-brittle multilayer. This particular geometry of the backstop is, on the other hand, common in natural cases. In cross-section, the model structural style is identical to previously published analogue models run with similar geometric, kinematic and dynamic parameters, and the box folds frequently bounded by forward and rearward thrust illustrated in Figs. 6B and 8A are characteristic of the deformation of a sandpack above a ductile substrate (Cotton and Koyi, 2000; Costa and Vendeville, 2002; Bahroudi and Koyi, 2003; Luján et al., 2003; Smit et al., 2003).

The originality of the presented models resides in the complex distribution of the structures in map view: the oblique structures developed throughout the model and were not located along transfer zones. Moreover, they formed at high angles or even nearly perpendicular to the structures defining the main structural trend, and they are particularly frequent in the models that are symmetrical with respect to the backstop movement (Models 90-45 and 120-30). The presence of a ductile layer at the bottom of the experimental multilayer is determinant for the development of such a complex structural pattern. Indeed, when the initial multilayer is composed only by brittle material, two monovergent thrust systems developed, rectilinear and parallel to the backstop sides (Figs. 6C and 9B). The formation of oblique structures had already been simulated in other types of analogue models, but: (a) the obliquity of the obtained structures was never so pronounced as that of the models presented in this paper, except in the cases of shortening produced by indenters; and (b) the structural patterns are very different in terms of spatial distribution of the oblique structures.

With a multilayer formed only by sand, Soto et al. (2002) performed a series of experimental wedges developed in a sandpack, with lateral and three-dimensional thickness variations. Marques and Cobbold (2002) studied the influence of erosion or sedimentation upon the development of thrust wedge – that is, entailing a high gradient of thickness of variation in the initial sandpack. In both cases, oblique structures developed, but the angle between mean trend and oblique structures was no higher than 40°. Calassou et al. (1993) show that the variations in basal friction and/or kinked backstop geometry control the development of transfer zones in thrust wedges. Nevertheless, the presence of oblique structures modelled by these authors is limited to these transfer zones,

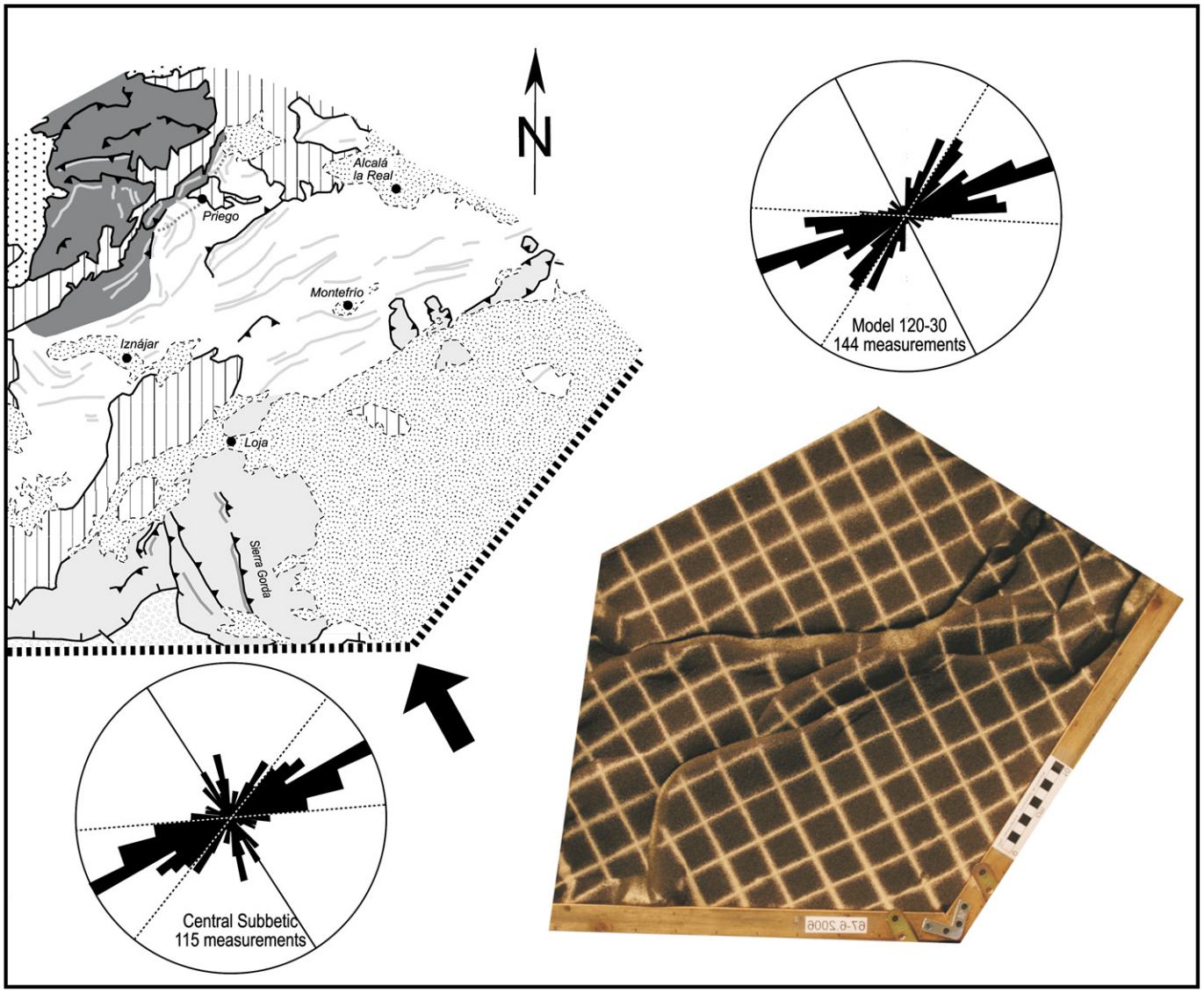


Fig. 10. Comparison between model and natural case in front of the recess drawn by the Alboran Domain outer boundary (drawn in thick dotted line). The final stage of Model 120-30 was reproduced as a mirror image and rotated to enhance the similarities. The rose diagram of Model 120-30 was constructed as those of Models 90-45, 90-22 and 120-0 (see legend in Fig. 6A). Total measurements, 144; largest petal, 17 values. The rose diagram labeled "Central Subbetic" corresponds to the measurements in the natural case, for the area appearing in the map. The dotted lines in the rose diagram represent the backstop side orientation, in both the model (imposed) and the natural case (deduced from geological mapping).

and the obliquity only reaches 40–50°. In light of the models presented in this paper, the results reached by Calassou et al. (1993) would have been very different if the initial sandpack had been floored by silicone.

Heterogeneities in the type – ductile or brittle – and thickness of the fold-and-thrust substrate can also produce oblique structures. Cotton and Koyi (2000) and Bahroudi and Koyi (2003) investigated the shortening of sandpack above adjacent ductile and frictional substrate in front of a straight backstop, with boundaries between ductile and frictional domains at the same time perpendicular to the backstop and parallel to its movement. Oblique structures in the sandpack developed in the area situated over the transition between domains: they show only 50° of obliquity, and they systematically end against a transfer fault zone. Luján et al. (2003) carried out experiments with different geometries of a ductile plate below a sand multilayer, in such a way that the movement of the backstop was oblique with respect to the frictional-viscous rear boundary. Angles of no more than 30° between main and oblique structures were observed. A thicker layer of ductile substrate below the sandpack is responsible for a farther propagation of the deformation front and can locally generate an arcuate thrust belt (Likorish et al., 2002). Finally, very complex structures including strike-slip faults and oblique structures, localized essentially along frictional-ductile substrate boundaries have been modelled recently by Storti et al. (2007) in experiments which involve along strike-tapered silicone floored multilayers.

The indenting of a backstop against either a brittle or a ductile-brittle multilayer produces structures whose pattern strongly depends on the geometry and movement direction of the indenter (Zweigel, 1998; Macedo and Marshak, 1999; Likorish et al., 2002; Crespo-Blanc and González-Sánchez, 2005). The presence of obstacles within the undeformed wedge can be included in this category of models (Marshak et al., 1992). Nonetheless, in all these models, the structural pattern of the resulting wedge generally consists of arcuate belts, in which domains with different orientations can be defined, the latter being oblique or nearly perpendicular. This is a quite different pattern than the one observed in the models presented here.

### 9.2. *Implications for the structural evolution of the central Subbetic fold-and-thrust belt*

The models presented in this paper were designed to study the influence of the recess marked by the Alboran Domain, i.e. the internal zones of the Betics, on the structural trend drawn by the paleomargin-derived external zones (Subbetic Domain). The Alboran Domain acted as a backstop that produced the shortening within the Subbetic units by a push-from-behind mechanism.

The presence of an evaporitic substrate in the Subbetic units imprints a structural style with a lack of preferred vergence, box folds, and pop-up and pop-down structures very similar to those simulated in the models. In fact, the cross-section A–A′ of the natural case (Fig. 4) is very similar to the model cross-section photograph of Fig. 6B. By contrast, the cross-section which illustrates the thrust system of Sierra Gorda shows a well-defined westward vergence (cross-section B–B′ of Fig. 4). Nevertheless, a thrust system developed over weak evaporites (that appear as a tectonic window below the sole thrust) may also show well-defined vergence, though limited to a wide domain. Such is the case of part of the Flysch Complex, in the westernmost Gibraltar Arc fold-and-thrust belt (Fig. 1; Luján et al., 2003).

In map view, the development of folds and thrusts in the analogue models shows a complex pattern in which the structures define a main structural trend, relative to which oblique structures are observed. This is qualitatively similar to the Subbetic fold-and-thrust belt that crops out in the central Betics. Moreover, Model 120-30 is quantitatively similar. In both the models and the natural case: (a) oblique structures are not located along transfer zones but are present everywhere, (b) this obliquity with respect to the structures that draw the main trend can reach 90°, and (c) the oblique structures are coetaneous with those drawing the main trend.

In order to enhance the similarities between the model and the central Subbetic natural case in terms of structure orientation variability, the final stage of Model 120-30 appears in parallel with the structural map of the central Betics in Fig. 10. The photograph of the model was reproduced as a mirror image with respect to Fig. 8. It was also rotated in such a way that the model backstop sides show an approximately similar orientation with respect to the Alboran Domain backstop recess deduced from mapping. Rose diagrams to quantify the orientation variations in both cases accompany the figure. The rose diagram for the Subbetic was constructed for the area that corresponds to the frontal part of the backstop, which in turn corresponds to the structural map of Fig. 10. Based on this map, the structural lines were divided into segments of 4 km length, according to the scaling factor between nature and model of $2 \times 10^5$, and their mean orientation was measured. One-third of the measurements in the Subbetic Domain are comprised between N60E and N85E (25° range), and two-thirds between N25E and N85N (60° range). Moreover, all the possible orientations are represented. On the whole, the orientation distribution represented by the rose diagram is very similar to that exhibited by Model 120-30.

Consequently, oblique structures within the ENE–WSW directed fold-and-thrust belt of the Subbetic Domain cropping our in the central Betics can adequately be explained in terms of oblique structures that developed in a deformed wedge floored by a ductile substrate of evaporitic rocks, in front of a recess marked by the outer boundary of the Alboran Domain (internal zones). It must be stressed that for the particular case of the Sierra Gorda oblique thrust system, other factors such as lateral variation of substrate (type and thickness) can be evoked, yet according to previous published models (Soto et al., 2002; Luján et al, 2003), these variations of parameters are not sufficient for producing structures subperpendicular to the main trend.

Finally, the possibility of generating oblique structures with a very high degree of obliquity with respect to the main trend during a single episode of shortening could be a key process in the complex evolution of the central Subbetic. Indeed, in this domain, superposed folding was described by Crespo-Blanc (2007). These interferences can be observed in the area of Alcalá la Real and Priego, that is, in front of the recess drawn by the Alboran Domain (Fig. 1). The relationships of the buckle-fold interference with syntectonic piggy-back sediments reveal that the folds of the first phase and those of the second one developed within a very short time span, if not simultaneously. Superposed buckle folding only arise when the trend of the pre-existing folds is nearly perpendicular to the later stress direction (Ghosh and Ramberg, 1968); if this angle is not higher than 80°, the earlier buckle folds tend to rotate, approaching the normal to the new shortening direction, instead of being overprinted by a second fold set (hinge migration of Odonne and Vialon, 1987). In the light of the analogue modelling presented in this paper, a working hypothesis concerning the origin of the superposed folding observed in the central Subbetic can be formulated. These interferences could generate from folds developed during the first stage of the shortening. If they were subperpendicular with the main trend, and assuming that their orientation was adequate (nearly parallel to the later shortening direction), they would have been refolded during the progressive deformation. This working hypothesis should now be tested through modelling with analogue materials that allow for the formation of superposed folding (Ghosh and Ramberg, 1968; Grujic et al., 2002; Sengupta et al., 2005).

## 10. Conclusions

1. In analogue modelling, a recess in a backstop can produce a complex pattern of structures, in which a main structural trend is accompanied by oblique structures. Such a pattern developed only if the multilayer showed a vertical rheological stratification consisting of a ductile substrate (silicone putty) situated below a brittle layer (sand).
2. The oblique structures developed everywhere in the models and were not located along discrete transfer zones.
3. In the models, both the structures that draw the main trend and the oblique ones developed simultaneously.
4. The grade of obliquity of the structural pattern is higher in models with recess sides oriented symmetrically with respect to the backstop movement. In the case of asymmetry, most of the structures developed subparallel to the side of the backstop that was at higher angle with respect to the backstop movement.
5. The natural case of the ENE–WSW trending fold-and-thrust belt of the central Subbetic shows remarkable similarities with one of the presented models (Model 120-30), in terms of cross-section, structural pattern and progressive deformation.
6. The origin of buckle-superposed folding observed in the central Subbetic may be related with folds developed during the first stage of the shortening, oriented subperpendicular to the main trend, then refolded when shortening proceeded.

## Acknowledgments

This study was supported by grants CGL2006-08638/BTE and CTM2005-08071-C03-01/MAR. We thank Jean Sanders for reviewing the English version. J.L. Simón and C. Faccenna are kindly acknowledged for their comments.

## References

Affolter, T., Gratier, J.P., 2004. Map view retrodeformation of an arcuate fold-and-thrust belt: the Jura case. Journal of the Geophysical Research 109, B03404, doi:10.1029/2002JB002270.

Bahroudi, A., Koyi, H.A., 2003. Effect of spatial distribution of Hormuz salt on deformation style in the Zagros fold and thrust belt: an anologue modeling approach. Journal of the Geological Society of London 160, 719–733.

Balanyá, J.C., García-Dueñas, V., 1988. El cabalgamiento cortical de Gibraltar y la tectónica de Béticas y Rif. In: Sociedad Geológica de España (Ed.), Actas Segundo Congreso Geológico de España (Simposios), Granada, pp. 35–44.

Balanyá, J.C., Crespo-Blanc, A., Díaz Azpiroz, M., Expósito, I., Luján, M., 2007. Structural trend line pattern and strain partitioning around the Gibraltar Arc accretionary wedge: insights as to the mode of orogenic arc building. Tectonics 26, TC2005, doi:10.1029/2005TC001932.

Berggren, W., Kent, D., Flynn, J., Van Couvering, J., 1985. Cenozoic geochronology. Geological Society of America Bulletin 96, 1407–1418.

Biju-Duval, B., Letouzey, J., Montadert, L., 1978. Structure and evolution of the Mediterranean basin. In: Proceeding ODP, Initial Report 42, pp. 951–984.

Bonini, M., 2001. Passive roof thrusting and forelandward fold propagation in scaled brittle-ductile physical models of thrust wedges. Journal of Geophysical Research 106 (B2), 2291–2311.

Calassou, S., Larroque, C., Malavieille, J., 1993. Transfer zones of deformation in thrust wedges: an experimental study. Tectonophysics 221, 325–344.

Comas, M.C., 1978. Sobre la geología de los Montes orientales: sedimentación y evolución paleogeográfica desde el Jurásico hasta el Mioceno inferior (Zona Subbética, Andalucía). Ph.D. thesis, Universidad del País Vasco.

Comas, M.C., García-Dueñas, V., Jurado, M.J., 1992. Neogene tectonic evolution of the Alboran Sea from MCS data. Geo-Marine Letters 12, 157–164.

Comas, M.C., Platt, J.P., Soto, J.I., Watts, A.B., 1999. The origin and tectonic history of the Alboran Basin: insights from Leg 161 results. In: Zahn, R., Comas, M.C., Klaus, A. (Eds), Proceedings of the Ocean Drilling Program, Scientific Results 161, pp. 555–580.

Corrado, S., Di Bucci, D., Naso, G., Faccenna, C., 1998. The influence of paleogeography on thrust system geometries: an analogue modelling approach for the Abruzzi-Molise (Italy) case history. Tectonophysics 296, 437–453.

Costa, E., Vendeville, B.C., 2002. Experimental insinghts on the geometry and kinematics of fold-and-thrust belts above weak, viscous evaporitic décollement. Journal of Structural Geology 24, 1729–1739.

Cotton, J., Koyi, H., 2000. Modeling of thrust front above ductile and frictional detachments: application to structures in the Salt Range and Potwar Plateau, Pakistan. Geological Society of America Bulletin 112/3, 351–363.

Crespo-Blanc, A., 2007. Superposed folding and oblique structures in the paleomargin-derived units of the Central Betics (SW Spain). Journal of the Geological Society of London 164/2, 621–636.

Crespo-Blanc, A., Campos, J., 2001. Structure and kinematics of the South Iberian paleomargin and its relationship with the Flysch Trough units: extensional reactivation within the Gibraltar Arc fold-and-thrust belt (western Betics). Journal of Structural Geology 23/10, 1615–1630.

Crespo-Blanc, A., González-Sánchez, A., 2005. Influence of indenter geometry on arcuate fold-and-thrust wedge: preliminary results of analogue modelling. Geogaceta 37, 11–14.

Davy, P., Cobbold, P.R., 1991. Experiments on shortening of a 4-layer model of the continental lithosphere. Tectonophysics 188, 1–25.

Díaz de Neira, J.A., Enrile Albir, A., Hernaiz Huerta, P.P., López Olmedo, F., Ruiz Reig, P., 1991. Geological map. Sheet Alcalá La Real, 990. Instituto Tecnológico Geominero de España, Madrid, scale 1:50'000.

Dercourt, J., et al., 1986. Geological evolution of the Tethys belt from the Atlantic to the Pamirs since the Lias. Tectonophysics 123, 241–315.

Durand-Delga, M., Rossi, P., Olivier, P., Puglisi, D., 2000. Situation structurale et nature ophiolitique de roches basiques jurassiques associées aux flyschs maghrébins du Rif (Maroc) et de Sicile (Italie). Comptes-Rendus de l'Académie des Sciences de Paris. Earth and Planetary Sciences 331, 29–38.

Frizon de Lamotte, D., Andrieux, J., Guézou, J.C., 1991. Cinématique des chevauchements néogènes dans l'Arc bético-rifain: Discussion sur les modèles géodynamiques. Bulletin de la Société Géologique de France 162, 611–626.

Frizon de Lamotte, D., Crespo-Blanc, A., Saint-Bézar, B., Comas, M., Fernàndez, M., Zeyen, H., Ayarza,P., Robert-Charrue, C., Chalouan, A., Zizi, M., Teixell, A., Arboleya, M.-L., Alvarez-Lo'bato, F., Julivert, M., Michard A., 2004. TRANSMED-transect I (Betics, Alboran Sea, Rif, Moroccan Meseta, High Atlas, Jbel Saghro, Tindouf basin): a description of the section and data sources. In: Cavazza, W., Roure, F.M., Spakman, W., Stampfli, G.M., Ziegler, P.A. (Eds.), The TRANSMED Atlas: The Mediterranean Region from Crust to Mantle. ISBN: 3-540-22181-6, CD-ROM.

Funiciello, F., Faccenna, C., Giardini, D., Regenauer-Lieb, K., 2003. Dynamics of retreating slabs: 2. Insights from three-dimensional laboratory experiments. Journal of Geophysical Research 108 (B4), 2207, doi:10.1029/2001JB000896.

García-Dueñas, V., Balanyá, J.C., Martínez-Martínez, J.M., 1992. Miocene extensional detachments in the outcropping basement of the northern Alboran Basin and their tectonic implications. Geo-Marine Letters 12, 88–95.

García-Hernández, M., López-Garrido, A.C., Rivas, P., Sanz de Galdeano, C., Vera, J.A., 1980. Mesozoic palaeogeographic evolution of the external zones of the Betic Cordillera. Geologie en Mijnbouw 59, 155–168.

Ghosh, S.K., Ramberg, H., 1968. Buckling experiments on intersecting fold patterns. Tectonophysics 5, 89–105.

Grujic, D., Walter, T., Gärtner, H., 2002. Shape and structure of (analogue models) of refolded layers. Journal of Structural Geology 24, 1313–1326.

Hindle, D., Burkhard, M., 1999. Strain, displacement and rotation associated with the formation of curvature in fold belts; the example of the Jura Arc. Journal of Structural Geology 21, 1089–1101.

Kley, J., 1999. Geologic and geometric constraints on a kinematic model of the Bolivian orocline. Journal of South American Earth Sciences 12, 221–235.

Koyi, H., 1988. Experimental modeling of role of gravity and lateral shortening in Zagros mountain Belt. The American Association of Petroleum Geologists Bulletin 72 (11), 1381–1394.

Likorish, W.H., Ford, M., Bürgisser, J., Cobbold, P.R., 2002. Arcuate thrust systems in sandbox experiments: a comparison to the external arcs of the Western Alps. Geological Society of America Bulletin 114, 1089–1107.

Lonergan, L., White, N., 1997. Origin of the Betic-Rif mountain belt. Tectonics 16/3, 504–522.

Luján, M., Storti, F., Balanyá, J.C., Crespo-Blanc, A., Rossetti, F., 2003. Role of décollement material with different rheological properties in the structure of the Aljibe thrust imbricate (Flysch Trough, Gibraltar Arc): an analogue modelling approach. Journal of Structural Geology 25, 867–881.

Lupiani, E., Soria, J.M., Baena, J., Pérez, A., 1988a. Geological map. Sheet Montefrío, 1008. Instituto Tecnológico Geominero de España, Madrid, scale 1:50'000.

Lupiani, E., Soria, J.M., Baena, J., Pérez, A., 1988b. Geological map. Sheet Loja, 1025. Instituto Tecnológico Geominero de España, Madrid, scale 1:50'000.

Macedo, J., Marshak, S., 1999. Controls on the geometry of fold-thrust belt salients. Geological Society of America Bulletin 111, 1808–1822.

Mansy, J.L., Manby, G.M., Averbuch, O., Everaerts, M., Bergerat, F., Van Vliet-Lanoe, B., Lamarche, J., Vandycke, S., 2003. Dynamics and inversion of the Mesozoic Basin of the Weald–Boulonnais area: role of basement reactivation. Tectonophysics 373, 161–179.

Marques, F.O., Cobbold, P.R., 2002. Topography as a major factor in the development of arcuate thrust belts: insights from sandbox experiments. Tectonophysics 348, 247–268.

Marshak, S., Wilkerson, M.S., Hsui, A.T., 1992. Generation of curved fold-thrust belts: insight from simple physical and analytical models. In: McClay, K.R. (Ed.), Thrust Tectonics. Chapman and Hall, London, pp. 83–92.

Odonne, F., Vialon, P., 1987. Hinge migration as a mechanism of superimposed folding. Journal of Structural Geology 9/7, 835–844.

Osete, M.L., Villalaín, J.J., Palencia, A., Osete, C., Sandoval, J., García-Dueñas, V., 2004. New palaeomagnetic data from the Betic Cordillera: constraints on the timing and the geographical distribution of tectonic rotations in Southern Spain. Pure and Applied Geophysics 161, 701–722.

Pineda, A., Ruiz P., 1983. Geological map. Sheet Archidona, 1024. Instituto Tecnológico Geominero de España, Madrid, scale 1:50'000.

Platt, J.P., Vissers, R.L.M., 1989. Extensional collapse of thickened continental lithosphere: a working hypothesis for the Alboran Sea and Gibraltar Arc. Geology 17, 540–543.

Rodríguez-Fernández, J., Sanz-de-Galdeano, C., 2006. Late orogenic intramontane basin development: the Granada Basin, Betics (southern Spain). Basin Research 18/1, 85–102.

Sengupta, S., Ghosh, S.K., Deb, S.K., Khan, D., 2005. Opening and closing of folds in superposed deformations. Journal of Structural Geology 27, 1282–1299.

Smit, J.H., Brun, J.P., Sokoutis, D., 2003. Deformation of brittle-ductile thrust wedges in experiments and nature. Journal of Geophysical Research 108 (B10), 2480.

Soto, R., Casas, A.M., Storti, F., Faccenna, C., 2002. Role of lateral thickness variations on the development of oblique structures at the Western end of the South Pyrenean Central Unit. Tectonophysics 350, 215–235.

Soto, R., Storti, F., Casas, A.M., Faccenna, C., 2003. Influence of along-strike pre-orogenic sedimentary tapering on the internal architecture of experimental thrust wedges. Geological Magazine 140/3, 253–264.

Storti, F., Soto, R., Rossetti, F., Casas Saínz, A., 2007. Evolution of experimental thrust wedge accreted from along-strike tapered, silicone-floored multilayers. Journal of the Geological Society of London 164, 73–85.

Vera, J.A., 2000. El Terciario de la Cordillera Bética: estado actual de conocimientos. Boletín de la Sociedad Geológica de España 13/2, 345–373.

Vera, J.A., 2004. Zonas externas Béticas. In: Vera, J.A. (Ed.), Geología de España. Sociedad Geológica de España-Instituto Geológico y Minero de España, pp. 354–389.

Villalaín, J.J., Osete, M.L., Vegas, R., García-Dueñas, V., Heller, F., 1994. Widespread Neogene remagnetization in Jurassic limestones of the South-Iberian palaeomargin (Western Betics, Gibraltar Arc). Physics of the Earth and Planetary Interior 85, 15–33.

Weijermars, R., Roep, T.B., Van den Eeckhout, B., Postma, G., Kleverlaan, K., 1985. Uplift history of a Betic fold nappe inferred from Neogene-Quaternary sedimentation and tectonics (in the Sierra Alhamilla and Almería, Sorbas and Tabernas Basin of the Betic Cordilleras, SE Spain). Geologie en Mijnbouw 64, 397–411.

Weijermars, R., Jackson, M.P.A., Vendeville, B., 1993. Rheological and tectonic modeling of salt provinces. Tectonophysics 217, 143–174.

Weijermars, R., Schmeling, H., 1986. Scaling of Newtonian and non-Newtonian fluid dynamics without inertia for quantitative modelling of rock flow due to gravity (including the concept of rheological similarity). Physics of the Earth Planetary Interior 43, 316–330.

Zweigel, P., 1998. Arcuate accretionary wedge formation at convex plate margin corners: results of sandbox analog experiments. Journal of Structural Geology 20, 1597–1609.